Available online at www.sciencedirect.com

jmr&t Journal of Materials Research and Technology

www.jmrt.com.br

Original Article

Structural and electrical properties of $Ca_{0.9}Dy_{0.1}MnO_3$ prepared by sol-gel technique.

K.R. Nandan[a,b], A. Ruban Kumar[b,*]

[a] Dept of Physis Jain University Bangalore Karnataka 562112, India.
[b] Center for Crystal Growth, VIT University, Vellore, Tamil Nadu, 632004, India

ARTICLE INFO

Article history:
Received 19 March 2017
Accepted 25 May 2017
Available online 31 May 2019

Keywords:
Sol–gel
Structural
Dielectric properties
Electrical properties
Impedance spectroscopy

ABSTRACT

In the present study, we have discussed about the synthesis of $Ca_{0.9}Dy_{0.1}MnO_3$ by using citric acid as a chelating agent. Structural and morphological studies were carried out by using XRD, FT-IR, FE-SEM equipped with EDX for the synthesized material. Magnetic studies are carried out by VSM and confirmed the paramagnetic behavior. The electric properties like dielectric, impedance and conductivity is carried out at the frequency range of 50 Hz to 5 MHz for different temperatures. Impedances studied for the activation energy and the investigation of grain and grain boundary effects. The conductivity studies were explained on the basis of Jonscher's power law and the activation energy is calculated.

1. Introduction

Rare earth manganites have received a remarkable attention due to the rich physical phenomenon and its potential applications in magnetic data storage, fuel cells, sensors, microwave devices because of the magnetic interaction playing an important role in producing magnetoelectric effects [1]. In manganites, the electronic structure due to the close relationship between the bond length of Mn and O atoms, the charge and spin–orbital ordering exhibits a large magnetoresistive property which significantly improves by doping and also by the synthesis method [2,3].

$CaMnO_3$ is a manganese-based compound which is having good applications has cathode materials in fuel cells, magnetoresistance switching's, the thermoelectric material at high temperature and excellent dielectric absorbing agent [3]. $CaMnO_3$ exhibit low electrical conductivity which affects electronic devices to overcome this issue by doping perovskite with rare earth elements ($Ca_{1-x}Re_xMnO_3$, Re: rare earth element) have been leading has an exciting behavior on their physical and chemical properties makes of promising magnetic, electronic materials and improves the electrical conductivity due to charge mismatch and increasing the Mn^{3+} Mn^{4+} ratio which helps to enhance the electron mobility and thermoelectric performances [4].

The low concentration of rare earth elements shows huge changes in the thermoelectric properties. Some studies showed that lanthanide elements doping at the Ca site is an effective way to improve the thermoelectric properties in $CaMnO_3$. The doping of Dy at Ca site causes a

* Corresponding author.
E-mail: arubankumarvit@gmail.com (A.R. Kumar).
https://doi.org/10.1016/j.jmrt.2017.05.020

dramatic improvement in the thermoelectric properties which are reported nowadays in thermoelectric materials to have an enormous interest because of conversion of heat into electricity directly [5,6]. The thermoelectric materials are potential candidates in automobiles and other similar sources at high temperature because of its high chemical stability and less harmful effects in materials [7]. The material has low dimensionality and quantum confinement in the nano range synthesized materials which shows a fascinating electrical, optical and magnetic properties compare to a bulk material [8].

Usually, the most of the studies carried out only on the magnetic, thermoelectric, properties of $CaMnO_3$, less attention has been paid to learn about the conductivity, resistivity and impedance properties of material. An impedance study is a very convenient and powerful tool for the correlation of electrical properties of the material. The present focus of this study is to analyze the dielectric, impedance and conductivity properties of the small amount of Dy doped at $CaMnO_3$.

2. Experimental

$Ca_{0.9}Dy_{0.1}MnO_3$ (CDMO) perovskite was synthesized by sol–gel method using citric acid as a chelating agent. The starting materials were of analytical grade and used were without further purification to synthesize CDMO, the reagents are calcium nitrate tetrahydrate ($Ca(NO_3)_2{\cdot}4H_2O$), dysprosium nitrate hydrate ($Dy(NO_3)_3{\cdot}6H_2O$), manganese nitrate tetrahydrate ($Mn(NO_3)_3{\cdot}4H_2O$) and citric acid ($C_6H_8O_7$) as a chelating agent. All the reagents are dissolved in the millipore water to form homogenous solution. The chelating agent citric acid solution was added slowly drop by drop to the metallic solutions with continuous stirring to ensure homogeneity continuously for 3 h at room temperature. The homogenous solution is heated at 80 °C to evaporate the water molecule until it forms the gel. The obtained gel was dried overnight in a vacuum oven at 130 °C. It was then pre-sintered at 300 °C in air for 4 h to eliminate the organic constituents presents by decomposition. Finally, the precursor was sintered at 800 °C for 5 h to obtain the final product. Again the obtained final product was ground into fine powder before subjecting it into further characterization.

2.1. Material characterization

The final product was subjected to various characterization techniques. The phase formation was confirmed by X-ray diffraction (XRD, Brucker D8 Advance, Cu Kα radiation, $\lambda = 1.5406$ Å with the 2θ range from 10° to 80° with step size of $0.02\,S^{-1}$ at scan rate of $2\,min^{-1}$. The Fourier transform infrared spectroscopy (FT-IR) spectra were obtained by JASCO 400 Infrared spectrometer from 4000 to 400 cm^{-1}. The surface morphology and compositions of the samples were investigated by Field emission scanning electron microscopy (Carl Zeiss EVO-185H, UK) equipped with an energy-dispersive X-ray spectrometer (EDX). The room temperature magnetic measurement was analyzed by vibrating sample magnetometer (VSM, Lakeshore VSM 7410) up to 15 kOe applied magnetic field. The synthesized powder was converted to cylindrical pellets for electrical measurements by coating with silver paste for ohmic contact. The dielectric analysis was measured by using an LCR meter (HIOKI 3532-50 LCR meter HITESTER) in the frequency range from 50 Hz to 5 MHz for temperature ranging from 373 K to 523 K.

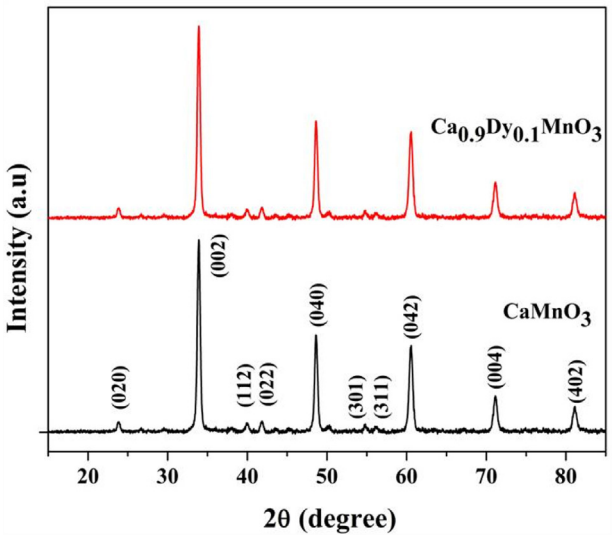

Fig. 1 – XRD pattern of $CaMnO_3$ and $Ca_{0.9}Dy_{0.1}MnO_3$ samples.

3. Results and discussion

3.1. XRD analysis

Fig. 1 illustrates the XRD pattern of nanocrystalline $CaMnO_3$ (CMO) and $Ca_{0.9}Dy_{0.1}MnO_3$ (CDMO) materials calcined at 800 °C. All the patterns of the prepared material confirmed without any measurable impurity phases indicating that a single phase of the orthorhombic structure with the space group *Pnma*. There is no secondary phases were observed from the synthesized material. From the doped and undoped sample shows that the doped ions do not change the crystalline structure of the material. The obtained diffraction peaks were indexed with the standard *h k l* values by confirming with JCPDS card number 89-0666. The lattice parameters and volume of the synthesized materials is found to be $a = 5.279$ Å, $b = 7.470$ Å, $c = 5.281$ Å and 208.25 Å respectively by using the powderX software [9]. The unit cell volume of CDMO slightly increases compared to CMO, such increase may be due to the radius of Dy^{3+} ions which are smaller than that of Ca^{2+} ions, and the doping of Dy will induce a creation of charge carrier ratio of Mn^{3+} in the Mn^{4+} matrix, the ionic radius of the Mn^{3+} ion is larger than that of Mn^{4+} ion [10]. The crystallite size was calculated from the major peaks of XRD pattern by using the following Scherrer's formula:

$$S = \frac{0.9\lambda}{\beta \cos\theta} \quad (1)$$

where λ the wavelength of the Cu-Kα radiation (1.5406 Å) and β is the full-width half maxima (FWHM) of the XRD peaks and θ

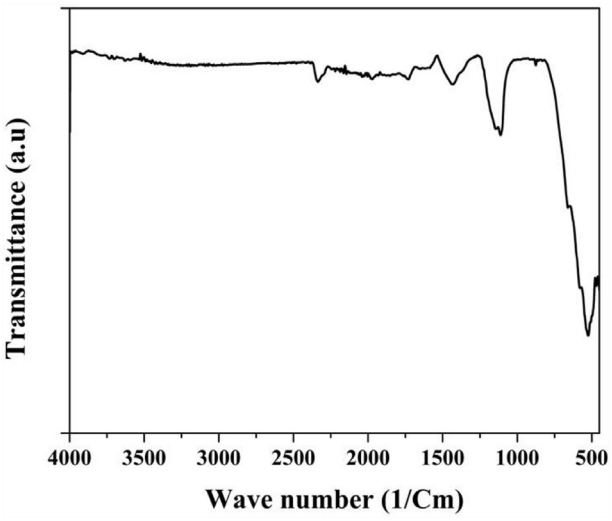

Fig. 2 – FT-IR spectra of $Ca_{0.9}Dy_{0.1}MnO_3$.

is the Bragg's angle. The average crystallite size was calculated to be in the range of 17–32 nm.

3.2. *FT-IR spectroscopy*

Fig. 2 shows the FT-IR spectra of the as-prepared $Ca_{0.9}Dy_{0.1}MnO_3$ sample. The bands obtained at 560 cm^{-1} corresponds to the stretching vibrational mode of the Mn—O—Mn or Mn—O bonds and the bending mode at around 410 cm^{-1} corresponds to changes in the bond angle of Mn—O—Mn. The bands at 1420 cm^{-1} show that metal cations complexes and the wide 570 cm^{-1} absorption band of calcinated sample at around 800 °C suggests the formation of perovskite structure. The absence of any other absorption bands at higher regions of wave number confirms the absences of other bands related to organic materials used during preparation of the material [11,12].

3.3. *FESEM-EDX*

The surface morphology and EDX spectrum are shown in Fig. 3. From the FSEM images, we clearly observed the well-defined grains and grain boundaries. The grains have an average size in between 200 and 300 nm. From the EDX spectrum shows the chemical composition spectra along with the percentage of each element, and it confirms the absence of any other impurity in the prepared material shows the exact formation of the composition.

3.4. *Magnetic studies*

Fig. 4 shows the magnetic properties of the synthesized CDMO at room temperature are carried out by using vibrating magnetometer (VSM). The perovskite CMO exhibits antiferromagnetic behavior at room temperature whereas the prepared Dy substituted CMO material at room temperature shows paramagnetic behavior from the *M–H* graph observed in

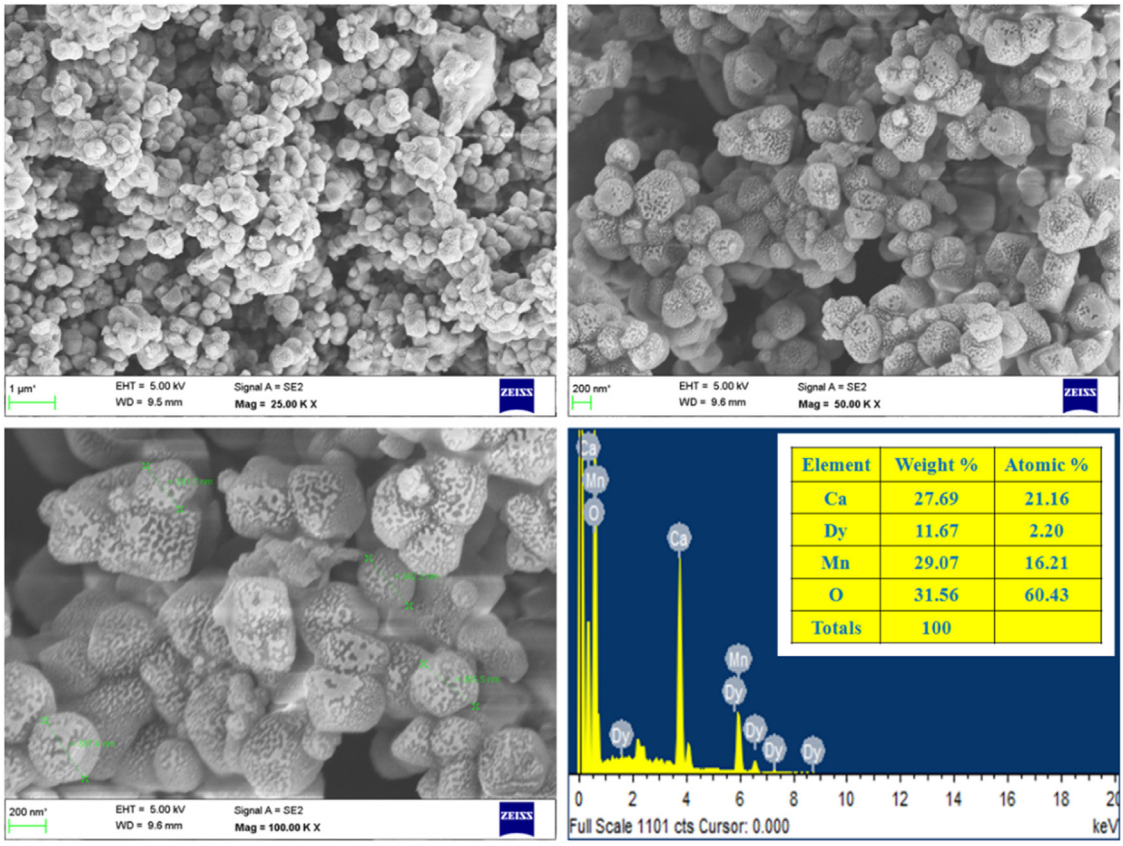

Fig. 3 – FE-SEM images of different magnifications and EDX of CDMO.

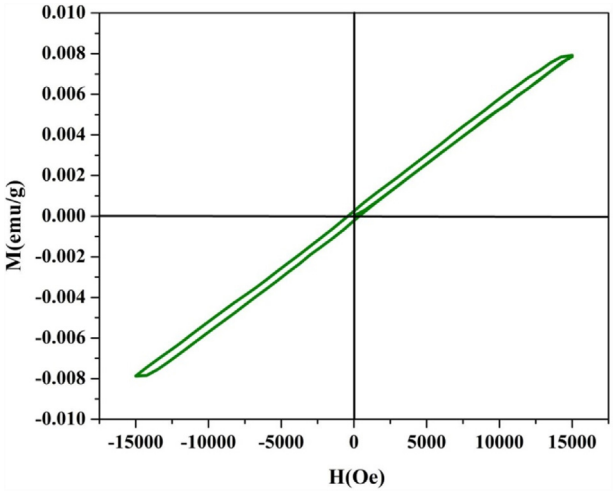

Fig. 4 – Hysteresis loop at room temperature of CDMO.

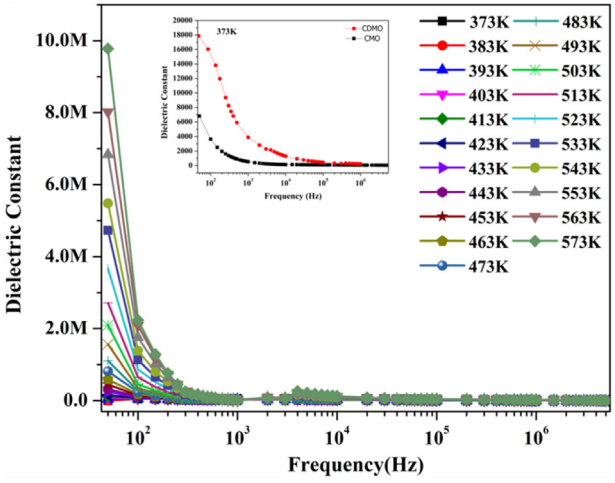

Fig. 5 – Variation of dielectric constant with frequencies of CDMO.

Fig. 4. This transition from antiferromagnetic to paramagnetic behavior signifies to the disturbing magnetic domain ordering with the increasing thermal energy which is more than the exchange interaction mechanism energy [3]. The obtained various magnetic parameters from VSM are magnetization (M_s), retentivity (M_r) and coercivity (G) of CDMO are 7.8954×10^{-3} emu, 234.12×10^{-6} emu and 391.78 G respectively.

3.5. *Dielectric studies*

The dielectric constant (ε') have been analyzed at the frequency ranging from 50 Hz to 5 MHz at the temperature ranging from 373 K to 523 K for the pellets. The following equation calculates the dielectric constant:

$$\varepsilon' = \frac{Cd}{A\varepsilon_0} \tag{2}$$

where C represents capacitance in farad, d represents the thickness of the pellet in mm, and A represents the cross-sectional area of the pellet in mm. Fig. 5 shows the variation of

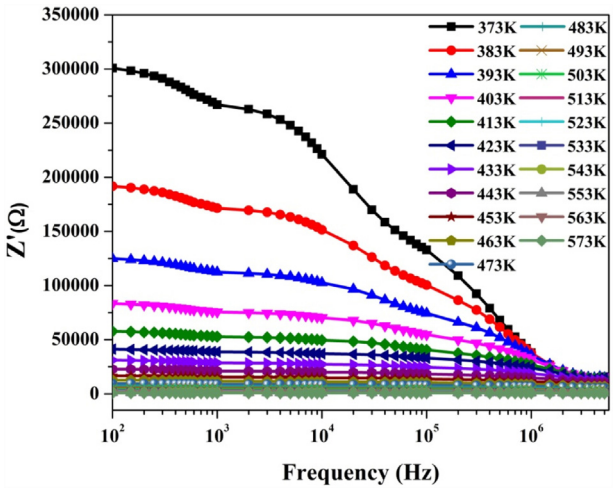

Fig. 6 – Variation of Z′ with frequency for different temperatures.

temperature and frequency dependent of dielectric constant. The value of dielectric constant decrease with increasing frequency is due to the charge carriers cannot follow the applied electric field beyond certain frequency range; it shows dielectric constant is almost independent of the frequency in the high-frequency region. This type of behavior can be explained by Maxwell–Wargner relaxation which is used in most of the microwave printed circuit board applications [13]. The higher value of dielectric constant is observed at the lower frequency is due to the presence of space charge polarization or interfacial polarization in the material. Usually, the dielectric constant dispersion below the frequency 10^2 Hz is associated with the space charge polarization. The lower value of dielectric constant is observed at higher frequencies which are very much useful in the ferroelectric, photonic and electro-optic device fabrication. From inset Fig. 5 it is observed that the minute doping of Dy it improves the dielectric constant at the particular temperature.

3.6. *Impedance studies*

Fig. 6 shows the variation of real part of impedance as a function of frequency at different temperatures. The value of impedance varies with both frequencies and as well as temperature. The pattern observed in the low-frequency region is almost followed by a saturation region. The decreasing in the value of Z' with increasing in frequency suggests the presence of negative temperature coefficient of resistance which makes the enhancement of the immobile species in the prepared material [14]. During the high frequency region, the value of Z' tends to merge; this shows a possibility of increasing ac conductivity with the rise in temperature. This indicates the release of the presence of space charge and reduction in the barrier properties of the prepared material [15].

Fig. 7 illustrates the frequency dependence of imaginary part of impedance (Z'') for various temperatures. These plots clearly show that the presence two asymmetric peaks with different relaxation frequency in the lower temperatures and after that a single peak occur. The peak shift toward

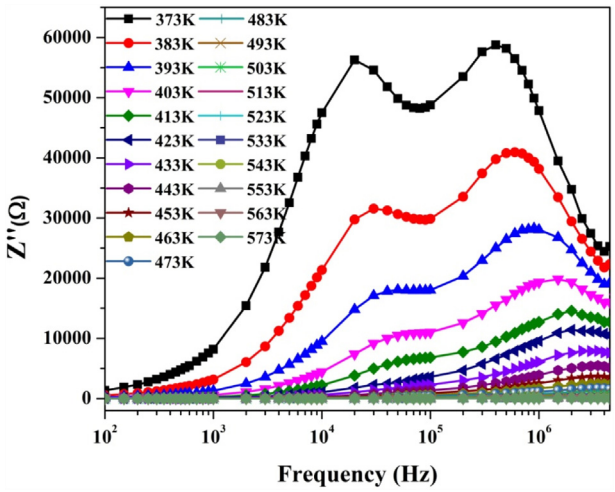

Fig. 7 – Variation of Z″ with frequency for different temperatures.

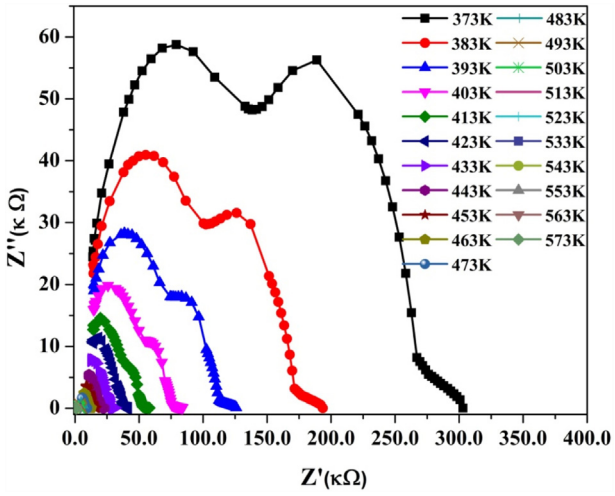

Fig. 8 – Nyquist plots of impedance data for different temperatures of CDMO.

the higher frequency region with the rise in temperature signifying the temperature dependent relaxation phenomenon [16]. The peaks height is directly related to resistance of phases present in the grain and grain boundaries. The relaxation process occurs due to the presence of immobile charge carriers, and occurrence of oxygen vacancy at the variation in the oxidation states [17]. The obtained results show good agreement with complex impedance spectra.

Complex impedance spectra at different temperature for CDMO are shown in Fig. 8. It is one of the essential techniques to investigate the electrical properties with the individual contribution from the grains, grain boundaries and interface effects. Fig. 8 represents the appearance of two overlapped semicircles, this exhibits some remarkable variation in the conduction mechanism. The presence of two semicircular shows the presence of two different relaxation times of grain and grain boundaries in the material. The arcs in

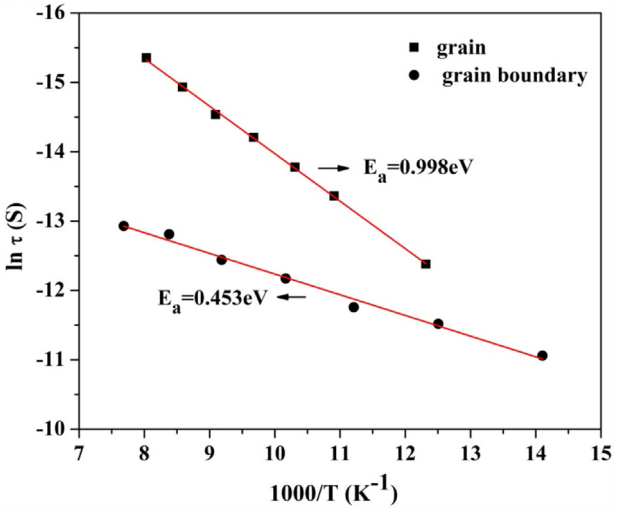

Fig. 9 – Arrhenius plot of temperature dependence of relaxation time of CDMO.

the low-frequency and high-frequency region showed the contributions from the grain boundary and grain region respectively. Further increase in temperature, two semicircular arcs appear in the form of a single semicircular arc denoting the dominance of grain effect over grain boundaries effect. The diameters of both semicircular arcs are directly related with the resistivity of two grain, and grain boundaries phase [18]. As the temperature increases an arc attached to the semicircle at lower frequency side denoting the existence of electrode interface conduction. The diameter of both semicircle decrease suggests semiconducting nature if the increase in the semicircular arcs attributes to the metallic nature [17]. The resistance in the grain is more at a lower temperature, as it decreases with increase in the temperature and conductivity increases.

Fig. 9 shows the activation energy determined from the Arrhenius plot for the grain and grain boundary effect separately for the prepared material. The obtained activation energy for grain is 0.453 eV and grain boundary is 0.998 eV. The obtained values predict the conduction inside grain has low energy compared to the grain boundaries which influences the existence of oxygen vacancy due to the defects, migration of electrons at the grain boundaries and also the hopping mechanism of Mn [19].

3.7. *Conductivity*

The transport properties for the CDMO for temperature dependent ac conductivity is obtained from the dielectric response data given by

$$\sigma_{ac} = \omega\varepsilon'\varepsilon_0 \tan\delta \quad (5)$$

Fig. 10 shows the variation of frequency versus the ac-conductivity at different temperatures for CDMO. From the conductivity graph it clearly shows the three regions, one is the dispersion in the low frequency region, plateau region and dispersion at high frequency region. From the graph, it

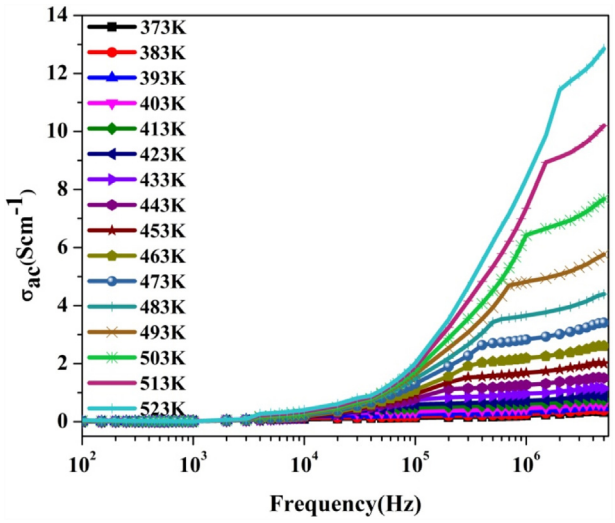

Fig. 10 – Frequency dependent ac-conductivity of CDMO for different temperatures.

clearly observed at low frequency region the conductivity is independent of the frequency which shows dc-conductivity and the dispersion at high frequency region correspond to ac-conductivity. The increasing frequency value of ac conductivity increases due to the disordering of cations between adjacent sides and also by the presence of space charge effect [20]. The dispersion gets narrowed as increasing frequency of the conductivity which increases with increasing temperature which shows the thermally activated phenomenon.

Fig. 11(a) shows the variation of frequency versus ln(σ) at lower temperature range from 373 K to 573 K fitted with the Jonscher's power law. The plateau obtained at the lower frequency domain and at the higher frequency domain corresponds to the electrode polarization effect and it obeys the Jonscher's power law.

$$\sigma(\omega) = \sigma_0 + A\omega^n \quad (6)$$

where σ_0 represents the dc conductivity which is the frequency independent plateau obtained in the low frequency region, A represents the pre-exponential factor and n represents the fraction exponential factor which has a value of 0–1 indicating the diffusion limited hopping pathway and ideal long-range pathways respectively. From the Jonscher's power law we could observe the deviation from dc conductivity value at low frequency region due to the electrode polarization. In the prepared material the value of conductivity is maximum at higher temperatures and higher frequency corresponds to the temperature dependent thermal mechanism phenomenon this occurs due to the influence of charge carriers [21]. In the lower frequency and temperature range the value of conductivity is low due to the presence of active grain boundary because of the delay in the mobile charge carriers. The value of σ_0, A and n obtained from Jonscher's power law is a universal property of materials it is related to the hopping mechanism using power law the fitted values are tabulated in Table 1. Table 1 shows the functional change in the frequency

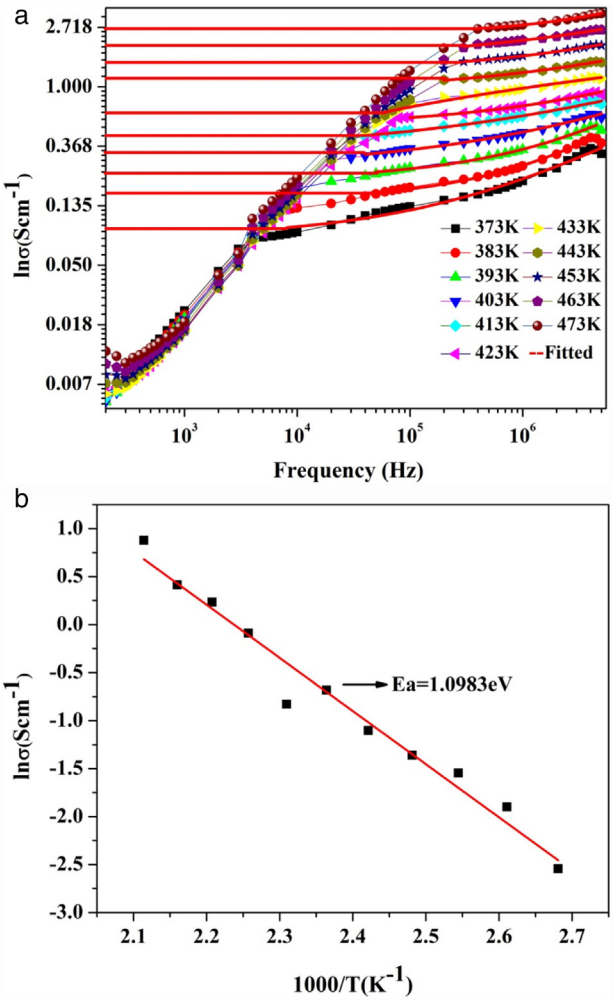

Fig. 11 – (a) Variation of frequency versus σ_{ac} conductivity fitted with Jonscher's power law for different temperatures and (b) Arrhenius behavior of dc conductivity ln(σ) versus 1000/T from frequency dependent conductivity for different temperature.

independent of dc conductivity and frequency dependent of ac conductivity of the prepared material. The total conductivity of the sample is the combination of dc and ac conductivity. According to power law the frequency dependent conductivity lies in the relaxation phenomenon this arises due to mobile charge carriers. The n value obtained from Jonscher's power law signifies to the translation motion of charge carrier with sudden hopping mechanism for $n<1$ and localized hopping mechanism for $n>1$ for the conduction mechanism due to the thermal activation [22]. The activation energy from the Arrhenius least fit for dc conductivity data obtained to be 1.098 eV which is shown in Fig. 11(b). The obtained value of activation energy is being to hopping mechanism of electrons, presence of oxygen vacancy and defects in the prepared material at high temperature [23].

Table 1 – Fitted data of Jonscher's power law of CDMO.

T (K)	σ_{dc} (S cm^{-1})	A (S cm^{-1} rad^{-n} s^{-1})	n
373	0.07864	2.49E−04	0.45504
383	0.14989	3.21E−05	0.56328
393	0.21289	7.04E−05	0.54779
403	0.25657	0.00133	0.3663
413	0.33162	0.00465	0.29714
423	0.43678	3.93933	0.39127
433	0.50536	9.87E−04	0.2205
443	0.91493	0.00265	0.35407
453	1.26347	0.00195	0.3879
463	1.51274	0.00871	0.31412
473	2.40773	1.83E−04	0.55946

4. Conclusion

The $Ca_{0.9}Dy_{0.1}MnO_3$ was synthesized by sol–gel method using citric acid as the chelating agent. The synthesized material was subjected to XRD and FT-IR for structural confirmation, and FE-SEM equipped with EDX for the morphological images and chemical compositions. The transition of aniferromagnetic behavior of CMO to paramagnetic behavior of CDMO was confirmed by VSM studies. Maxwell–Wargner relaxation was observed from dielectric measurement. Nyquist plot showed the grain and grain boundary effects, and the semicircular arcs appear in the form of a single semicircular arc denoting the dominance of grain effect over grain boundaries effect. The grain boundaries in the synthesized material influenced in the existence of oxygen vacancy due to the defects, migration of electrons at the grain boundaries and also the hopping mechanism of Mn. Conductivity measurements were explained by using Jonscher's power law. The activation energies obtained for the material is due to hopping mechanism of electrons, presence of oxygen vacancy and defects in the prepared material at high temperature.

Conflicts of interest

The authors declare no conflicts of interest.

Acknowledgments

The authors would like to thank Dr. S. Kalainathan for providing dielectric facilities and also the VIT University for their constant encouragement and support.

REFERENCES

[1] Alqat A, Gebrel Z, Spasojević V, Kusigerski V, Bošković S, Blanuša J. Influence of the particle size reduction on magnetic properties of electron-doped $Ca_{1-x}Y_xMnO_3$. Nucl Technol Radiat Protect 2012;27(4):351–4, http://dx.doi.org/10.2298/NTRP1204351A.

[2] Negi P, Dixit G, Agrawal HM, Srivastava RC. Structural, optical and magnetic properties of multiferroic $GdMnO_3$ nanoparticles. J Supercond Nov Magn 2013;26(5):1611–5, http://dx.doi.org/10.1007/s10948-012-1870-0.

[3] Kompany A, Ghorbani-Moghadam T, Kafash S, Abrishami ME. Frequency dependence of Néel temperature in $CaMnO_{3-\delta}$ ceramics: synthesized by two different methods. J Magn Magn Mater 2014;349:135–9, http://dx.doi.org/10.1016/j.jmmm.2013.08.015.

[4] Liu CJ, Bhaskar A, Yuan JJ. High-temperature transport properties of $Ca_{0.98}RE_{0.02}MnO_{3-\delta}$ (RE = Sm, Gd, and Dy). Appl Phys Lett 2011;98(21):214101, http://dx.doi.org/10.1063/1.3003065.

[5] Zhu Y, Wang C, Wang H, Su W, Liu J, Li J. Influence of Dy/Bi dual doping on thermoelectric performance of $CaMnO_3$ ceramics. Mater Chem Phys 2014;144(3):385–9, http://dx.doi.org/10.1016/j.matchemphys.2014.01.006.

[6] Zhu YH, Su WB, Liu J, Zhou YC, Li J, Zhang X, et al. Effects of Dy and Yb co-doping on thermoelectric properties of $CaMnO_3$ ceramics. Ceram Int 2015;41(1):1535–9, http://dx.doi.org/10.1016/j.ceramint.2014.09.089.

[7] Bhaskar A, Liu CJ, Yuan JJ. Thermoelectric properties of $Ca_{1-x}Gd_xMnO_{3\delta}$ (0.00, 0.02 and 0.05) systems. Sci World J 2012, http://dx.doi.org/10.1100/2012/149670.

[8] Negi P, Dixit G, Agrawal HM, Srivastava RC. Structural, optical and magnetic properties of multiferroic $GdMnO_3$ nanoparticles. J Supercond Nov Magn 2013;26(5):1611–5, http://dx.doi.org/10.1007/s10948-012-1870-0.

[9] Dong C. PowderX: Windows-95-based program for powder X-ray diffraction data processing. J Appl Crystallogr 1999;32(4):838.

[10] Zhan B, Lan J, Liu Y, Lin Y, Shen Y, Nan C. High temperature thermoelectric properties of Dy-doped $CaMnO_3$ ceramics. J Mater Sci Technol 2014;30(8):821–5, http://dx.doi.org/10.1016/j.jmst.2014.01.002.

[11] Nandan KR, Kumar AR. Electrical properties of $Ca_{0.925}Ce_{0.075}Mn_{1-x}Fe_xO_3$ ($x = 0.1–0.3$) prepared by sol–gel technique. J Mater Sci Mater Electron 2016;27(12):13179–91, http://dx.doi.org/10.1007/s10854-016-5464-7.

[12] Kljaljević M, Jordanov L, Stoiljković D, Kusigerski M, Spasojević V, Matović VB. Effects of sintering on the structural, microstructural and magnetic properties of nanoparticle manganite $Ca_{1-x}Gd_xMnO_3$ ($x = 0.05, 0.1, 0.15, 0.2$). Ceram Int 2015;41(10):14964–72, http://dx.doi.org/10.1016/j.ceramint.2015.08.041.

[13] Balamurugaraj P, Suresh S, Koteeswari P, Mani P. Growth, optical, mechanical, dielectric and photoconductivity properties of L-proline succinate NLO single crystal. J Mater Phys Chem 2013;1(1):4–8, http://dx.doi.org/10.12691/jmpc-1-1-2.

[14] Jacob R, Nair HG, Isac J. Impedance spectroscopy and dielectric studies of nanocrystalline iron doped barium

strontium titanate ceramics. Process Appl Ceram 2015;9(2):73–9, http://dx.doi.org/10.2298/PAC1502073J.
[15] Thakur S, Rai R, Bdikin I, Valente MA. Impedance and modulus spectroscopy characterization of Tb modified $Bi_{0.8}A_{0.1}Pb_{0.1}Fe_{0.9}Ti_{0.1}O_3$ ceramics. Mater Res 2016;19(1):1–8, http://dx.doi.org/10.1590/1980-5373-MR-2015-0504.
[16] Lobo LS, Kalainathan S, Kumar AR. Investigation of electrical studies of spinel $FeCo_2O_4$ synthesized by sol–gel method. Superlattices Microstruct 2015;88:116–26, http://dx.doi.org/10.1016/j.spmi.2015.09.010.
[17] Ur Rahman A, Rafiq MA, Maaz K, Karim S, Oh Cho S, Hasan MM. Temperature induced delocalization of charge carriers and metallic phase in $Co_{0.6}Sn_{0.4}Fe_2O_4$ nanoparticles. J Appl Phys 2012;112(6):063718, http://dx.doi.org/10.1063/1.4754559.
[18] Chauhan L, Shukla AK, Sreenivas K. Dielectric and magnetic properties of nickel ferrite ceramics using crystalline powders derived from DL alanine fuel in sol–gel auto-combustion. Ceram Int 2015;41(7):8341–51, http://dx.doi.org/10.1016/j.ceramint.2015.03.014.
[19] Wang CC, Lei CM, Wang GJ, Sun XH, Li T, Huang SG, et al. Oxygen-vacancy-related dielectric relaxations in $SrTiO_3$ at high temperatures. J Appl Phys 2013;113(9):094103, http://dx.doi.org/10.1063/1.4794349.
[20] Singh NK, Kumar P, Rai R, Kholkin AL. Structural and impedance spectroscopy analysis of $Ba(Fe_{0.5}Nb_{0.5})O_3$–$BaTiO_3$ ceramic system. Adv Mater Lett 2012;3(4):315–20, http://dx.doi.org/10.1016/j.ssc.2008.10.026.
[21] Lakhdar MH, Larbi T, Ouni B, Amlouk M. AC conductivity, dielectric relaxation and modulus behavior of Sb_2S_2O new kermesite alloy for optoelectronic applications. Mater Sci Semicond Process 2015;40:596–601, http://dx.doi.org/10.1016/j.mssp.2015.07.019.
[22] Naceur H, Megriche A, El Maaouli M. Frequency dependant dielectric characteristics and conductivity behavior of $Sr_{1-x}(Na_{0.5}Bi_{0.5})_xBi_2Nb_2O_9$ ($x = 0.0$, 0.2, 0.5, 0.8, and 1.0) ceramics. Orient J Chem 2013;29(3):937–44.
[23] Kool A, Thakur P, Bagchi B, Hoque NA, Banerjee S, Das S. Sol–gel synthesis of transition-metal ion conjugated alumina-rich mullite nanocomposites with potential mechanical, dielectric and photoluminescence properties. RSC Adv 2015;5(126):104299–313, http://dx.doi.org/10.1039/C5RA21091G.